Regular Article

Check for
updates

Dynamics of nonlinear optical rectification, second, and third harmonic generation in asymmetric triangular double quantum wells due to static electric and magnetic fields

E. B. Al, E. Kasapoglu, F. Ungan[a]

Department of Physics, Faculty of Science, Sivas Cumhuriyet University, 58140 Sivas, Turkey

© The Author(s), under exclusive licence to Società Italiana di Fisica and Springer-Verlag GmbH Germany, part of Springer Nature 2022

Abstract In this study, we present a theoretical simulation of the impact of applied external electric and magnetic fields on the nonlinear optical rectification (NOR), second harmonic generation (SHG), and third harmonic generation (THG) in typical $GaAs/Ga_{0.6}Al_{0.4}As$ asymmetric double triangular quantum wells. At first, we have calculated the wave functions and the subband energy levels for the lowest bounded four states confined within the structure by solving the Schrödinger equation using the diagonalization method within the framework of the effective mass and single parabolic band approximations. Then, the analytical expressions of the NOR, SHG, and THG are obtained using compact density matrix approach via iterative method. According to the numerical results, it is concluded that electric and magnetic fields play a vital and important role in the electronic and optical properties of the system and they can be used to adjust the intersubband transitions and change the associated optical sensitivities.

1 Introduction

Recently, thanks to the continuous improvement in technology, the growth of various types of low-dimensional semiconductor structures (LDSSs) such as quantum well (QW), quantum well wire (QWW) and quantum dot (QD) has been achieved [1–6]. Due to the strong quantum confinement of carriers, such structures offer electronic and optical properties as desired, allowing optoelectronic devices to have a wider range of applications. Compared to other structures, QWs with larger band gaps have been studied in detail in different situations, as it is easier to grow, process and convert them into usable devices. Also, the physical properties of QWs can be controlled and adjusted as desired by using different compositional profiles and by changing the shape of the well with the external fields. Therefore, the electronic and optical properties in semiconductor QW structures have received considerable attention, and these properties have been investigated in various semiconductor QW structures in various studies [7–15].

Theoretical investigation of electromagnetic field effects on the electronic and optical properties of LDSSs can have very important consequences for potential applications. For this reason, many studies have been carried out in this context and as a result of these studies, it has been shown that the energies and related wave functions are significantly changed for an electron confined in various quantum structures under electric and magnetic fields [16–23].

The linear intersubband absorption within the conduction band of a $GaAs$ QW has been studied experimentally with and without an electric field [24–26]. A very large dipole strength and a narrow bandwidth have been observed, which suggest that the intersubband optical transition in QWs may have huge nonlinearities. Theoretical results reveal that the linear and nonlinear intersubband absorptions significantly depend on the structure of the system and the applied electric field [11,27–29]. The second-order susceptibility is negligible except for the small contribution of the bulk susceptibility in symmetric QWs. As known, when the inversion symmetry of a system is broken, it is possible to obtain remarkable nonlinear properties. Asymmetric structures can be created, either by advanced material growing technology or by an external applied electric field. Gurnick and DeTemple obtained asymmetric QW with asymmetric composition gradients of Al in the growth direction for $GaAlAs$ material, and they found $10-100$ times larger values than those of bulk materials of the second-order nonlinearities for a Morse potential [30,31] and observed a larger second-order susceptibility than that of the bulk case in $GaAs$ QWs with the effect of the electric field. Results reveal a significant enhancement of nonlinear properties with the increasing electric field. The potential chosen in this study has a tunable asymmetry degree and therefore is expected to yield promising nonlinear optical properties.

As can be seen, the optical properties have been investigated in QWs with various geometries, and double triangle QWs (TQWs) are one of them. Zhao et al. [32] have studied the absorption coefficients (ACs) and THG in single and double TQWs. The ACs and relative refractive index changes for various double QW shapes such as rectangular, triangular and parabolic have been theoretically

[a] e-mail: fungan@cumhuriyet.edu.tr (corresponding author)

Springer

studied by Silotia et al [33] under an applied external magnetic and laser fields. Chen et. al. studied the ACs [34], NOR [35], and SHG [36] in ADTQWs.

However, optical properties under the influence of electric and magnetic fields were not considered in ATDQWs separated by a thin barrier layer. Therefore, in the present study, we theoretically examine SHG and THG as well as NOR in such a structure under the influence of electric and magnetic fields. Optical properties related to subband transitions are calculated in a density matrix approximation, and energy calculations are based on the diagonalization method in the effective mass and single parabolic band approximations. This paper is divided as follows: in Sect. 1, the theoretical equations which are used to obtain the optical properties of the structure are located in detail. In Sect. 2, the obtained results and discussions are shown. A summary of the physical results is given in the final section.

2 Theory

In this present section, we will explain how calculate the impact of static electric and magnetic fields on the electron subband energy levels and their corresponding wave functions in the ATDQWs, and will present the formalism for the NOR, SHG, and THG coefficients. For this, we will consider a $GaAs/Ga_{0.6}Al_{0.4}As$ ATDQWs with the wells of widths Lw_L and Lw_R are separated by a thin barrier of width L_B. The growth direction of the structure is the z-axis. In the effective-mass and parabolic band approximations, the Hamiltonian for an electron confined in the structure under the presence of an static magnetic field-$\mathbf{B}$ ($\mathbf{B} = (B, 0, 0)$ is applied perpendicular to the growth direction (x-axis)) and static electric field-$\mathbf{F}$ ($\mathbf{F} = (0, 0, F)$ is applied directed along the z-direction)) is given by

$$H = -\frac{1}{2m^*}\left(\mathbf{P} + \frac{e}{c}\mathbf{A}(\mathbf{r})\right)^2 + V(z) + |e|Fz, \tag{1}$$

where m^* is the electron effective mass, $\mathbf{P}$ is the momentum operator, e is the electronic charge of an electron, c is the speed of light in free space, the Landau gauge $\mathbf{A}(\mathbf{r}) = -Bz\hat{y}$, F is the strength of the applied electric field, and $V(z)$ is the electron confinement potential given by [37],

$$V(z) = \begin{cases} V_0, & z < -Lw_L - L_B/2, \\ \frac{-z - L_B/2}{Lw_L}V_0, & -Lw_L - L_B/2 < z < -L_B/2, \\ V_0, & -L_B/2 < z < L_B/2, \\ \frac{z - L_B/2}{Lw_R}V_0, & L_B/2 < z < Lw_R + L_B/2, \\ V_0, & z > Lw_R + L_B/2 \end{cases} \tag{2}$$

where V_0 is the band discontinuity and calculated by $V_0 = 0.6(1155x + 370x^2)$ meV, where x is the Al concentration in the barrier regions, Lw_L is the left QW width, Lw_R is the right QW width, and L_B is the central barrier width.

In order to calculate the effect of static electric and magnetic field on the NOR, SHG, and THG coefficients of GaAs/Ga$_{1-x}$Al$_x$As ATDQWs, the energy eigenvalues and eigenfunctions of the structure are obtained from the solution of Eq. (1) using the diagonalization method [38]. After finding the electron subband energies and their corresponding envelope wave functions, we can employ the analytical expressions for the NOR, SHG and THG coefficients derived within the compact density matrix approach as described in Refs. [39]. These are, respectively;

$$\chi_0^{(2)} = \frac{4e^3\sigma_v}{\varepsilon_0\hbar^2}\mu_{01}^2\,\delta_{01}\,\frac{\omega_{10}^2(1 + \Gamma_2/\Gamma_1) + (\omega^2 + \Gamma_2^2)(\Gamma_2/\Gamma_1 - 1)}{\left[(\omega_{10} - \omega)^2 + \Gamma_2^2\right]\left[(\omega_{10} + \omega)^2 + \Gamma_2^2\right]}, \tag{3}$$

$$\chi_{2\omega}^{(2)} = \frac{e^3\sigma_v}{\varepsilon_0\hbar^2}\,\frac{\mu_{01}\,\mu_{12}\,\mu_{20}}{(\omega - \omega_{10} - i\,\Gamma_3)(2\omega - \omega_{20} - i\,\Gamma_3)}, \tag{4}$$

$$\chi_{3\omega}^{(3)} = \frac{e^4\sigma_v}{\varepsilon_0\hbar^3}\,\frac{\mu_{01}\,\mu_{12}\,\mu_{23}\,\mu_{30}}{(\omega - \omega_{10} - i\,\Gamma_3)(2\omega - \omega_{20} - i\,\Gamma_3)(3\omega - \omega_{30} - i\,\Gamma_3)}. \tag{5}$$

Here, σ_v is the electron density in the structure, ε_0 is the dielectric permittivity of the vacuum, $\hbar$ is the reduced Planck constant, $\mu_{ij} = \langle\psi_i|z|\phi_j\rangle$, $(i, j = 0, 1, 2)$ is off-diagonal matrix elements, and $\delta_{10} = |\mu_{00} - \mu_{11}|$, $\omega_{ij} = (E_i - E_j)/\hbar$ is the transition frequency, $\Gamma_k = 1/T_k$ with $k = (1, 2, 3)$ indicates the relaxation rate.

3 Results and discussion

In this section, the effect of static electric and magnetic fields on the NOR, SHG and THG coefficients in a $GaAs/Ga_{1-x}Al_xAs$ ADTQW will be discussed. The physical parameters used in the our calculations are [40]: $m^* = 0.067m_0$ where m_0 is the single electron bare mass, $e = 1.602 \times 10^{-19}$ C, $\hbar = 1.056 \times 10^{-19}$ Js, $Lw_L = 15$ nm, $Lw_R = 20$ nm, $L_B = 2$ nm, $\varepsilon_0 = 8.854 \times 10^{-12}$ C^2/Nm^2, $\sigma_v = 3.0 \times 10^{22}$ m^{-3}, $V_0(x = 0.40) = 312.72$ meV, $\Gamma_1 = 1.0$ THz, $\Gamma_2 = 5.0$ THz, and $\Gamma_3 = 7.0$ THz.
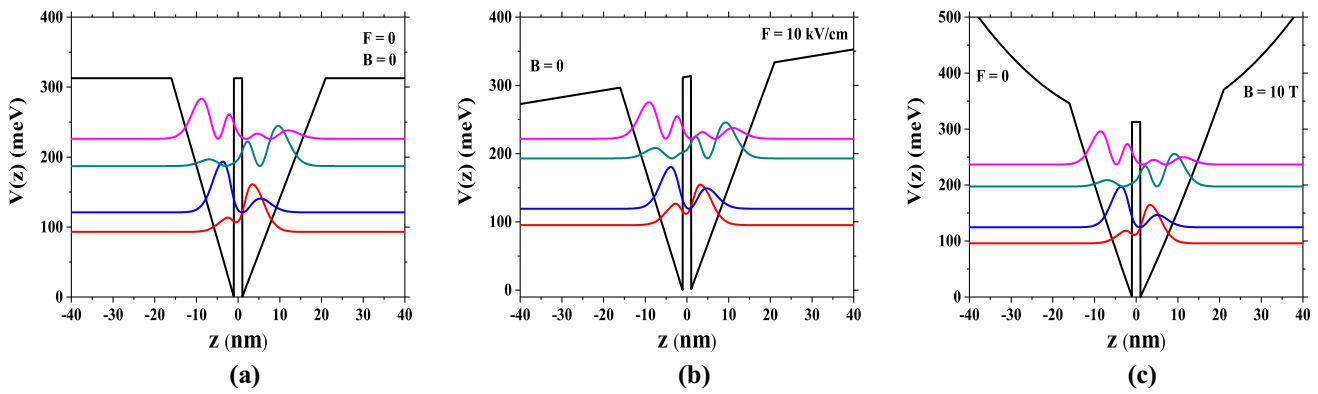
Fig. 1 The confinement potential profiles and electron probability densities of an asymmetric triangular quantum well system: **a** $F = 0$, $B = 0$, **b** $F = 10 kV/cm$, $B = 0$, and **c** $F = 0$, $B = 10T$

In Fig. 1, we present the confinement potential, the first four energy levels, and the probability densities of the respective electronic levels in the absence and presence of electric and magnetic fields. The figure corresponds to (a) the absence of electric and magnetic field, (b) the presence of electric field and absence of magnetic field, and (c) the presence of magnetic field and absence of electric field. The maximum probability densities for all cases are located in the well regions, which means that the electron is confined in the $GaAs$ region. Because within the potential barriers, the wave functions vanish. However, as a result of the tunneling effect caused by the barrier at the center, the probability densities are formed as follows: (i) For the ground state, the first maximum of the probability density is in the right well and the second maximum is in the left well. (ii) For the 1st excited state, the first maximum of the probability density is in the left well and the second maximum is in the right well. (iii) For the 2nd excited state, the first and second maximums of the probability density are in the right well, and the third maximum is in the left well. (iv) For the 3rd excited state, the first and second maximums of the probability density are in the left well, and the third and fourth maximums are in the right well. As can be seen from Fig. 1b, with the application of the electric field in the z-direction, the structure is twisted counterclockwise and the probability density of the electron for all levels decreases in the right well and increases in the left well. Thus, while the energies of the even states (E_0 and E_2) increase, the energies of the odd states (E_1 and E_3) decrease. Because with the increase in the electric field, the left well expands and its lower value decreases, but the right well narrows and its lower value increases, which decreases the energies of the states localized in the left well and increases the energies of the states localized in the right well. In Fig. 1c, we can see the extra parabolic confinement created by the magnetic field. While this extra parabolic confinement does not cause a significant change on the probability densities of the electron, it makes a positive contribution to the Hamiltonian as shown in Eq. 1, causing an increase in all energies in the structure. However, it should be noted that while the upper states are more affected by the magnetic field, the energy increase due to the magnetic field toward the lower states decreases due to the shielding of the magnetic field by the upper states.

The optical coefficients given by Eqs. 3, 4 and 5 depend on the transition energy and the corresponding matrix element. Therefore, to better understand the behavior of intersubband optical properties under electric and magnetic fields, we first graph the transition energies and matrix elements as functions of electric and magnetic field. To examine the transition energies in the ATDQW system, in Fig. 2, we present the main transition energies as a function of electric field and magnetic field for constant values of $Lw_L = 15 nm$, $Lw_R = 20 nm$, and $L_B = 2 nm$. As seen in Fig. 2a, with the increase in the electric field, while the $E_1 - E_0$ and $(E_3 - E_0)/3$ transition energies decrease, $(E_2 - E_0)/2$ transition energy increases. The reason for this is the changes in the energies, as we mentioned above, due to the twisting in the structure with the application of the electric field. Thus with increasing electric field; i) $E_1 - E_0$ transition energy decreases because E_1 decreases while E_0 increases, ii) $(E_2 - E_0)/2$ transition energy increases because the increase in E_2 is greater than E_0 and iii) $(E_3 - E_0)/3$ transition energy decreases because E_0 increases while E_3 decreases. When we look at Fig. 2b, we see that all transition energies increase with increasing magnetic field because, as we mentioned above, the upper levels are more affected by the magnetic field, they show a larger increase with the increase in the magnetic field compared to the ground state. Also, as can be seen from the order of magnitude of the subband transition energies, all the results obtained will relate to optical processes in the far infrared region (FIR) of the spectrum.

Figure 3 shows the dependence of the product of the respective transition matrix elements in the optical coefficients on the electric and magnetic fields. As seen in the figure, with increasing electric and magnetic field, while the product terms in NOR and SHG decrease, the product term in THG increases.

Figure 4 shows the calculated NOR coefficient as a function of incident photon energy for applied external three different electric and magnetic field values. NOR is a Lorentzian-like function which, as stated in Eq. 3, depends on the $E_1 - E_0$ transition energy, the μ_{01} dipole matrix element, the average electron displacement (δ_{01}) associated with the transition, and the frequency of the incident light (ω). Other quantities in the equation are constant parameters. We observe that the peak position of the NOR coefficient in Fig. 4a exhibits a redshift because the $E_1 - E_0$ transition energy decreases with the increase in the electric field as seen in Fig.

Fig. 2 The variations of the main transition energy differences as a function of incident photon energy for three different values of **a** static electric field and **b** static magnetic field
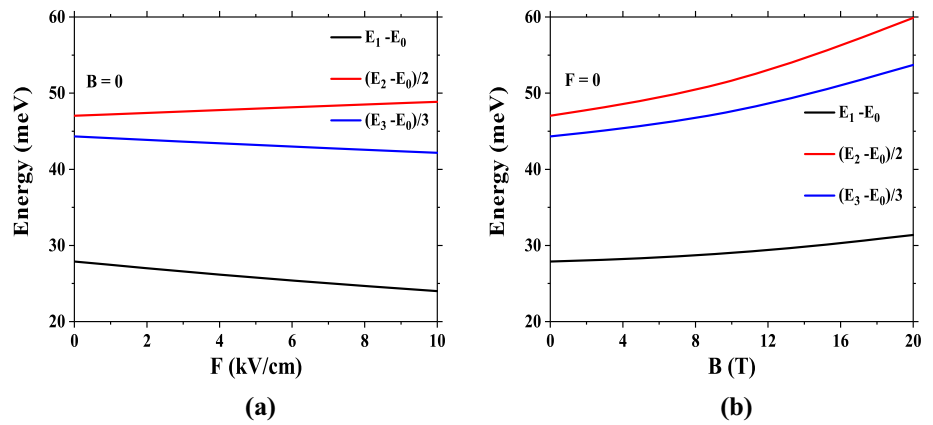
2a. Moreover, when the magnitude of magnetic field increases, it is seen that the $E_1 - E_0$ transition energy increases (see Fig. 2b) as the confinement potential becomes stronger and as a result, the peak position of the NOR coefficient shifts to blue (Fig. 4b). It can be easily noted from Eq. 3 that the magnitude of the resonance peak of NOR is proportional to the product $\mu_{01}^2 \, \delta_{01}$. As can be seen from Fig. 3a and b, this product value decreases with the increase in the electric and magnetic fields and accordingly the peak amplitude of the NOR coefficient decreases.

In Fig. 5, the SHG coefficient is plotted as a function of incident photon energy for three different electric and magnetic field values. Two prominent resonance peaks of the SHG coefficient appear in the figures. The larger one occurs around $\hbar\omega = (E_2 - E_0)/2$, and the smaller one occurs around $\hbar\omega = E_1 - E_0$. As can be noted in Fig. 5a, as the magnitude of electric field increases, the larger resonance peak shows blueshift, while the smaller resonance peak shows redshift, and thus they are separated from each other and at the same time the peak values decrease because, as can be noted from Fig. 2a, the magnitude of electric field increases, $(E_2 - E_0)/2$ transition energy increases, while $E_1 - E_0$ transition energy decreases, and at the same time, it is shown in Fig. 3a that the product of three dipole matrix elements ($\mu_{01} \, \mu_{12} \, \mu_{20}$) related to SHG also decreases with increasing electric field. Similarly, Figure 5b shows us that both the larger and smaller resonance peaks undergo a distinct blueshift with the increase in the magnetic field because, as noted in Fig. 2b, $E_1 - E_0$ and $(E_2 - E_0)/2$ transition energies increase as the magnetic field increases. Since the $(E_2 - E_0)/2$ transition energy increases faster than the $E_1 - E_0$ transition energy, the larger and smaller peaks move away from each other as the magnetic field increases. In addition, this figure further shows us that both the larger resonance peak and the smaller one decrease rapidly with the increase in the magnetic field. We can also attribute the amplitude decrease to the fact that the product of the three dipole matrix elements ($\mu_{01} \, \mu_{12} \, \mu_{20}$) associated with SHG in Fig. 3b decreases with increasing magnetic field. As a result, the applied external electric and magnetic fields can be suitable parameters to adjust the resonance peak positions and amplitudes of SHG.

Figure 6 shows the THG coefficient as a function of incident photon energy for different electric and magnetic field values. In fact, when we look at Eq. 5, we can easily say that the THG coefficient should have three resonance peaks and the position of these three resonance peaks should be approximately $\hbar\omega = E_1 - E_0$, $\hbar\omega = (E_2 - E_0)/2$, and $\hbar\omega = (E_3 - E_0)/3$. However, since the peak amplitude corresponding to $\hbar\omega = E_1 - E_0$ is very small, it is shown that there are only two resonance peaks in Fig. 6a and b. In both figures, the maximum peak of THG coefficient corresponds to $\hbar\omega = (E_3 - E_0)/3$ transition energy. When only the electric field is taken into account (Fig. 6a), it is clear that the maximum resonance peak of THG coefficient shifts toward lower energy regions with the increasing electric field associated with the $(E_3 - E_0)/3$ transition energy in Fig. 2a. On the other hand, the second resonance peak shifts to higher energy regions with the increasing electric field associated with the $(E_2 - E_0)/2$ transition energy

Fig. 3 The variations of the dipole moment matrix elements as a function of incident photon energy for three different values of **a** static electric field and **b** static magnetic field
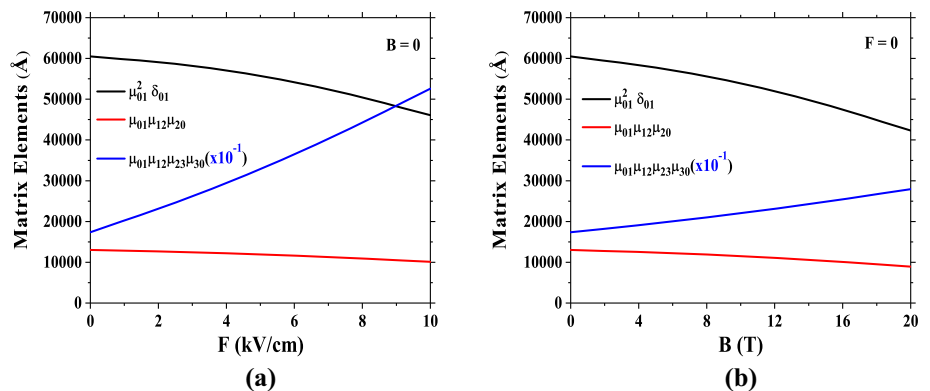
Fig. 4 The variations of NOR coefficients in the asymmetric triangular quantum well as a function of incident photon energy for three different values of **a** static electric field and **b** static magnetic field
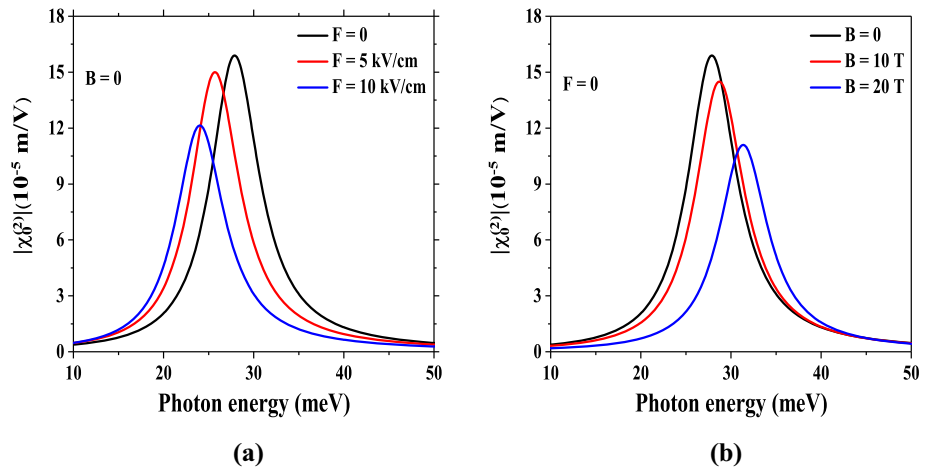

(a)

(b)

Fig. 5 The variations of SHG coefficients in the asymmetric triangular quantum well as a function of incident photon energy for three different values of **a** static electric field and **b** static magnetic field
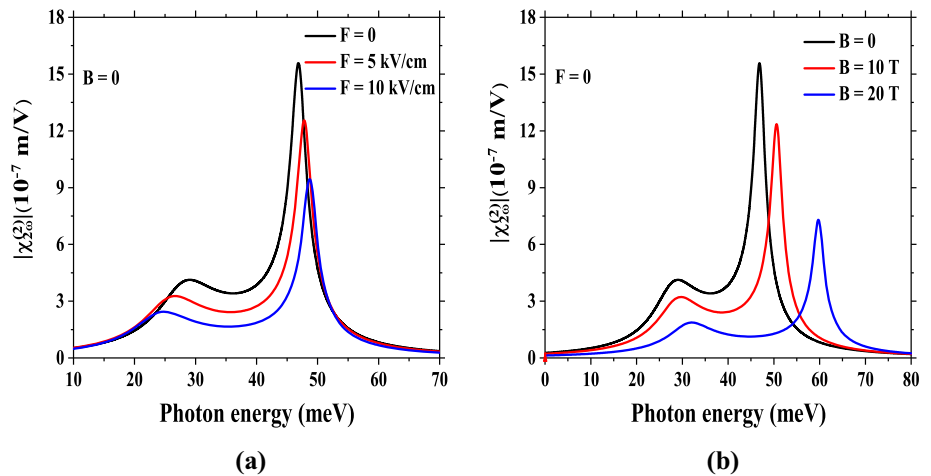

(a)

(b)

Fig. 6 The variations of THG coefficients in the asymmetric triangular quantum well as a function of incident photon energy for three different values of **a** static electric field and **b** static magnetic field
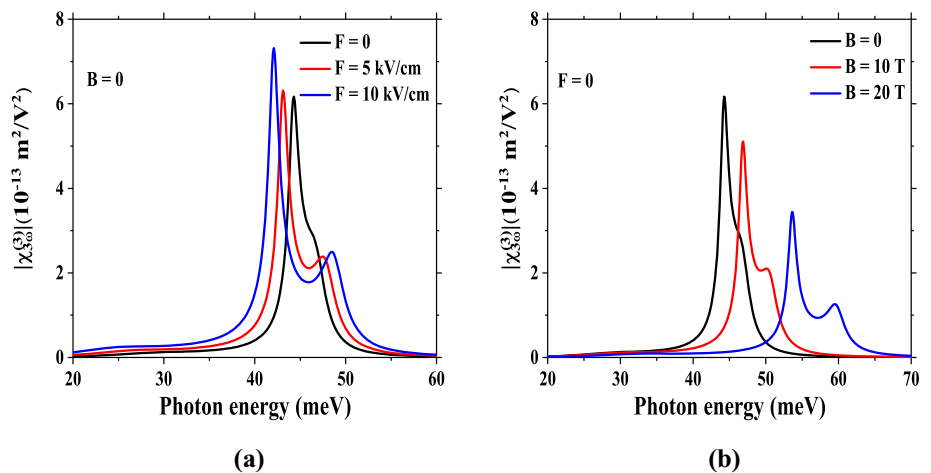

(a)

(b)

in Figure(a). This causes the distance between the first and second maximum amplitudes to increase as the electric field increases. Also, the peak values of THG coefficient increase with increasing electric field. This is because the product of the four dipole matrix elements ($\mu_{01}\,\mu_{12}\,\mu_{23}\,\mu_{30}$) increases smoothly due to the increasing electric field (Fig. 3a). Moreover, when only the magnetic field is taken into account in Fig. 6b, it is clear that the both resonance peaks of THG susceptibility shift toward higher energy regions with the increasing magnetic field associated with the transitions in Fig. 2b. In addition, the peak values of THG coefficient decrease monotonically with increasing magnetic field due to the change of the product of the four dipole matrix elements ($\mu_{01}\,\mu_{12}\,\mu_{23}\,\mu_{30}$) in Fig. 3b.

4 Conclusions

In the current study, a numerical investigation is performed to analyze the effect of electromagnetic fields on the NOR, SHG and THG coefficients in $GaAs/Ga_{0.6}Al_{0.4}As$ ATDQWs with finite confinement potential. Within the framework of effective mass and parabolic band approaches, the electron subband energies and their related wave functions are obtained by diagonalization method. It is found that the electric and magnetic fields change subband energies and they can be used to tune intersubband transitions. Moreover, the compact density matrix approximation is used to numerically examine the optical properties of ATDQWs. The results found in this context show the followings: (i) While the peak amplitude of the NOR coefficient decreases with increasing electric and magnetic field, the resonant peak position shifts to lower (higher) energies with increasing electric (magnetic) field. (ii) As the electric field increases, the peak amplitudes of the SHG coefficient decrease, while the maximum peak position shifts to higher energy and the second peak position shifts to lower energy. (iii) With increasing magnetic field, the peak amplitudes of the SHG coefficient decrease and the resonant peak positions shift to higher energies. (iv) With increasing electric field, while the maximum peak amplitude of THG decreases, the second peak amplitude first decreases and then increases, and the resonant peak positions shift to higher energies. (v) With increasing magnetic field, the peak amplitudes of the THG coefficient decrease and the resonant peak positions shift toward higher energies.

Consequently, the electric and magnetic fields can be used to shift the peak energy of optical coefficients, as well as changing their maximum values. Our numerical results may be useful to improve experimental studies of NOR, SHG and THG processes in LDSSs under electric and magnetic fields.

References

1. B. Zhang, H. Wang, X. Wang, Q. Wang, J. Fan, Y. Zou, X. Ma, J. Alloy. Comp. **872**, 159470 (2021)
2. E. Zielony, A. Wierzbicka, R. Szymon, M.A. Pietrzyk, E. Placzek-Popko, Appl. Surf. Sci. **538**, 148061 (2021)
3. M. Kappelt, V. Türck, M. Grundmann, H. Cerva, D. Bimberg, J. Cryst. Growth **170**, 590 (1997)
4. Y. Higuchi, S. Osaki, T. Kitada, S. Shimomura, Y. Takasuka, M. Ogura, S. Hiyamizu, Solid State Electron. **50**, 1137 (2006)
5. X. Yan, F. Tang, Y. Wu, B. Li, X. Zhang, X. Ren, J. Cryst. Growth **468**, 185 (2017)
6. S.R. Shriram, D. Panda, R. Kumar, J. Saha, B. Tongbram, M.R. Mantri, S.A. Gazi, A. Mandal, S. Chakrabarti, Opt. Mater. **114**, 110817 (2021)
7. H. Dakhlaoui, J.A. Vinasco, C.A. Duque, Superlatt. Microstruct. **155**, 106885 (2021)
8. S. Aqiqi, C.A. Duque, A. Radu, J.A. Vinasco, D. Laroze, Physica E **132**, 114763 (2021)
9. Y.H. Zan, S.L. Ban, Superlatt. Microstruct. **150**, 106782 (2021)
10. S. Mo, K. Guo, G. Liu, X. He, J. Lan, Z. Zhou, Thin Solid Films **710**, 138286 (2020)
11. F. Ungan, M.K. Bahar, J.C. Martinez-Orozco, M.E. Mora-Ramos, Photonics Nanostruct. **41**, 100833 (2020)
12. T. Hidouri, S. Nasr, F. Saidi, Optik **205**, 164253 (2020)
13. R. Arulmozhi, A.J. Peter, C.W. Lee, Chem. Phys. Lett. **742**, 137129 (2020)
14. C. Yu, F. Chen, L. Sun, H. Zhang, Optik **200**, 163440 (2020)
15. E.B. Al, F. Ungan, U. Yesilgul, E. Kasapoglu, H. Sari, I. Sökmen, Int. J. Mod. Phys. B **30**, 1650139 (2016)
16. A. Boda, Physica B **575**, 411699 (2019)
17. F. Ungan, S. Pal, M.E. Mora-Ramos, J.C. Martínez-Orozco, Optik **188**, 12 (2019)
18. J.A. Vinasco, A. Radu, R.L. Restrepo, A.L. Morales, M.E. Mora-Ramos, C.A. Duque, Opt. Mater. **91**, 309 (2019)
19. F. Ungan, H. Sari, E. Kasapoglu, U. Yesilgul, S. Sakiroglu, I. Sökmen, Photon. Nano. Fund. Appl. **32**, 47 (2018)
20. V.A. Holovatsky, I.V. Holovatskyi, M. Ya Yakhnevych, Physica E **104**, 58 (2018)
21. R.L. Restrepo, E. Kasapoglu, S. Sakiroglu, F. Ungan, A.L. Morales, C.A. Duque, Infrared Phys. Tech. **85**, 147 (2017)
22. R.L. Restrepo, F. Ungan, E. Kasapoglu, M.E. Mora-Ramos, A.L. Morales, C.A. Duque, Physica B **457**, 165 (2015)
23. Bin Li, Kang-Xian. Guo, Zuo-Lian. Liu, Yun-Bao. Zheng, Phys. Lett. A **372**, 1337 (2008)
24. A. Harwitt, J.S. Harris Jr., Appl. Phys. Lett. **50**, 685 (1987)
25. B.F. Levine, R.J. Malik, J. Walker, K.K. Choi, C.G. Bethea, D.A. Kleinman, J.M. Vandenberg, Appl. Phys. Lett. **50**, 273 (1987)
26. L.C. West, S.J. Eglash, Appl. Phys. Lett. **46**, 1156 (1985)
27. I. Altuntas, H. Dakhlaoui, M.E. Mora-Ramos, F. Ungan, EPJ Plus **136**, 1174 (2021)
28. F. Ungan, J.C. Martínez-Orozco, R.L. Restrepo, M.E. Mora-Ramos, Optik **185**, 881–887 (2019)
29. R.L. Restrepo, J.P. González-Pereira, E. Kasapoglu, A.L. Morales, C.A. Duque, Opt. Mater. **86**, 590–599 (2018)
30. M.K. Gurnick, T.A. DeTemple, IEEE J. Quantum Electron. **19**, 791 (1983)
31. M.M. Fejer, S.J.B. Yoo, R.L. Byer, A. Harwit, J.S. Harris, Phys. Rev. Lett. **62**, 1041 (1989)
32. Q. Zhao, S. Aqiqi, J.F. You, M. Kria, K.X. Guo, E. Feddi, Z.H. Zhang, J.H. Yuan, Physica E **115**, 113707 (2020)
33. P. Silotia, R. Giri, V. Prasad, Indian J. Pure Appl. Phys. **54**, 641 (2016)
34. B. Chen, K.X. Guo, R.Z. Wang, Z.H. Zhang, Z.L. Liu, Solid State Comm. **149**, 310 (2009)
35. B. Chen, K.X. Guo, R.Z. Wang, Y.B. Zheng, B. Li, Eur. Phys. J. B Condens. Matter **66**, 227 (2008)
36. B. Chen, K.X. Guo, R.Z. Wang, Z.H. Zhang, Superlattice. Microst. **45**, 125 (2009)
37. U. Yesilgul, J. Lumin. **132**, 765 (2012)
38. W. Xie, Y. Chen, Superlatt. Microstruct. **50**, 691 (2011)
39. R.W. Boyd, *Nonlinear Optics*, 3rd edn. (Rochester, New York, 2007)
40. F. Ungan, H. Sari, E. Kasapoglu, U. Yesilgul, S. Sakiroglu, I. Skmen, Photon. Nano. Fund. Appl. **32**, 47 (2018)